JOURNAL OF GEOPHYSICAL RESEARCH, VOL. 105, NO. A6, PAGES 13,017-13,028, JUNE 1, 2000

Evolution of thin current sheet with a southward interplanetary magnetic field studied by a three-dimensional electromagnetic particle code

K.-I. Nishikawa

Department of Physics and Astronomy, Rutgers University, Piscataway, New Jersey

S. Ohtani

Applied Physics Laboratory, Johns Hopkins University, Laurel, Maryland

Abstract. This paper reports the spatial and temporal development of sheet current intensification in the near-Earth tail using our three-dimensional global electromagnetic particle simulation with a southward turning interplanetary magnetic field (IMF) in a context of the substorm onset. As the solar wind with the southward IMF advances through the Earth, the near-Earth tail thins and the sheet current intensifies. The peak of the current density moves toward the Earth. Before its peak becomes maximum the reconnection takes place. The earthward flows are generated by the reconnection, which coincides with the earthward expansion of the intensified sheet current. Because of the pileup of the earthward plasma flows, the dawnward current is generated near the Earth. This dawnward current dissipates rapidly with the sheet current because of the opposite current direction, which coincides with the dipolarization in the near-Earth tail. This simulation study shows the sequence of the substorm dynamics in the near-Earth tail, which is similar to the features obtained by the multisatellite observations. The identification of the timing and mechanism of triggering substorm onset requires further studies in conjunction with observations.

1. Introduction

The solar wind interaction with the Earth's magnetic field gives rise to a number of important and intriguing phenomena, many of which are not fully understood because of their complex global nature. These include reconnection at the dayside magnetopause and in the magnetotail, flux transfer events, convection in the magnetosphere/ionosphere, and the generation of field-aligned current systems. One of the most important problems in the physics of the Earth's magnetosphere concerns the nature of the processes that occur in and near the magnetopause, cusps, flanks, and magnetotail, resulting in the transfer of solar wind mass and momentum into the interior of the cavity. These initiate a large-scale magnetospheric convection, which is related to substorms (e.g., *Lui* [1991], *Fairfield* [1992], and articles in the special section Magnetospheric Substorms: Invited Reviews in *Journal of Geophysical Research* (*101*(A6), 12,937-13,113, 1996) for recent reviews).

Observations suggest the formation of a thin current sheet with width $< 1\,R_E$ in the near-Earth region before the onset of the expansion phase [*Mitchell et al.*, 1990; *Sergeev et al.*, 1990; *Lui et al.*, 1992]. MHD ballooning instability has been investigated as a triggering mechanism [*Roux et al.*, 1991; *Ohtani and Tamao*, 1993; *Ma et al.*, 1995; *Samson et al.*, 1996]. However, *Ohtani et al.* [1998] found that both temporal and spatial scales of tail current disruption signatures are probably outside of, although could be at the marginal edge of, the ranges of the MHD approximation. Therefore, even though the global dynamics of the near-Earth substorm process may be simulated in the MHD framework [*Hesse and Birn*, 1991; *Birn and Hesse*, 1996], the kinetic treatment is essential for describing the tail current disruption.

Because of the importance of magnetic reconnection at the near-Earth magnetotail, theories and simulations with various methods have been performed extensively. The tearing instability in the magnetotail has been studied [e.g., *Schindler*, 1979; *Galeev and Zelenyi*, 1976]. The collisionless tearing instabilities are stabilized because of electron adiabaticity, which causes free energy otherwise available for the instability to be used up by plasma compression [*Lembège and Pellat*, 1982; *Pellat et al.*, 1991; *Pritchett*, 1994; *Pritchett and Büchner*, 1995]. Two-dimensional local particle simulations show the formation of a thin current sheet

Paper number 1999JA000215.
0148-0227/00/1999JA000215$09.00

with a deep minimum in the equatorial B_z field in the near-Earth magnetotail with the inductive electric field carried by a southward interplanetary magnetic field (IMF) [*Pritchett and Coroniti*, 1995]. Recently, three-dimensional (3-D) particle simulations indicate that the collisionless tearing instability grows rapidly because of the reduction of electron compressibility caused by the persistent drift kink mode (not included in single-fluid treatments) in the presence of a small B_z component [*Pritchett and Coroniti*, 1996; *Pritchett et al.*, 1996, 1997]. Furthermore, *Pritchett and Coroniti* [1997] show that highly east-west structured strong plasma flows can develop within the convectively driven plasma sheet because of the combined dynamical effects of reconnection and unstable interchange and kink modes for the case where magnetic flux is locked from leaving the region. Our global simulations [*Nishikawa*, 1997, 1998a, b] show this highly east-west structured strong plasma flow. *Nishikawa* [1998a, Plate 1] shows the evolution of the dawn-dusk structure of the electron density due to the drift kink instability in the dawn-dusk cross section near the reconnection region. These global simulations include effects from the dayside magnetopause, self-consistent stretched magnetic field by the solar wind with an IMF in the magnetotail, and particle entry from low-latitude boundary layers (flank) (especially, in the presence of the IMF B_y component) [e.g., *Rostoker*, 1996]. They are important for the magnetotail dynamics [e.g., *Baker et al.*, 1996; *Sergeev et al.*, 1996]. On the basis of the previous work, at the present time the drift kink mode instability seems to be a good candidate for the cross-field streaming instability; however, further investigation is necessary [*Daughton*, 1998, 1999; *Nishikawa*, 1997, 1998a].

It is essential to investigate the evolution of the thinned current sheet in order to understand instabilities that cause reconnection and associated phenomena such as earthward and tailward ion flows and dipolarization. *Hesse et al.* [1996] found that the major fraction of the enhanced current density in the thinned current sheet is supported by the electrons using a hybrid simulation. As will be described later, our 3-D electromagnetic (EM) particle simulations [*Nishikawa*, 1997, 1998a] show that the electrons are a major carrier in the thinned current sheet before the reconnection takes place (during the early growth phase). After the reconnection the ions become a major carrier near the Earth (later in the growth phase) [e.g., *Mitchell et al.*, 1990].

By investigating the dynamics of the thinned current sheet and earthward high-speed ion flows near the Earth one can gain a better understanding of the processes that control the substorm onset. Understanding the substorm onset is a challenging problem. Its solution is made difficult because of the variety of processes, regions, and scale length involved. We try to show in this paper that significant insight into these processes can be addressed with a new global particle method that includes full kinetic effects. This model makes major advances in that the electron motion and the ion motion are separately incorporated and each species is diagnosed according to the physics involved. Through the separation of the electron and ion dynamics, a more physical picture of the evolution of tail current, instability, magnetic reconnection, and substorm onset is attained and can be tested against observations.

Previously, we reported the simulation results with a southward IMF [*Nishikawa*, 1997, 1998a]. Here we summarize the previous report to describe the general guideline for this report. After a quasi-steady state is established with an unmagnetized solar wind at time step 768 we switch on a southward IMF, which causes the magnetosphere to stretch and allows particles to enter the cusps and nightside magnetosphere. Analysis of magnetic fields near the Earth confirms a signature of magnetic reconnection at the dayside magnetopause, and the plasma sheet in the near-Earth magnetotail clearly thins. Later, magnetic reconnection also takes place in the near-Earth magnetotail. Arrival of southward IMF near the front of the magnetosphere causes a sunward velocity in the dayside magnetosphere, as required to feed flux tubes into the dayside reconnection process. Sunward flow near the equatorial plane of the magnetosphere implies a dawn-to-dusk electric field. Initially, the velocity in the distant tail is not much affected by the southward turning. Therefore the dawn-dusk electric field increases in the sunward direction, which causes B_z to decrease with time in the near-Earth magnetotail. The cross-field current also thins and intensifies, which excites a kinetic (drift kink) instability along the dawn-dusk direction [*Nishikawa*, 1997, 1998a; *Daughton*, 1998, 1999]. Because of this instability the electron compressibility effect appears to be reduced and allows the collisionless tearing to grow rapidly with the reduced B_z component. Later, the nightside magnetic fields are dipolarized and a plasmoid is formed tailward. We find that because of the reconnection, particles are injected toward the Earth from the neutral line (X line) (D. S. Cai and K.-I. Nishikawa, Topological magnetic structure related to reconnection in the near-Earth magnetotail with southward IMF studied by three-dimensional electromagnetic particle code, submitted to *Geophysical Research Letteers*, 1999). In our simulations, kinetic effects self-consistently determine the dissipation rate in the magnetopause associated with reconnection.

Current disruption instabilities serve as the mesoscale or microscale internal processes to facilitate the transition from a tail-like to dipole-like field configuration in the plasma sheet [e.g., *Lui*, 1991]. The new conjecture suggests that the near-Earth magnetotail is an important region for the substorm trigger [*Mukai et al.*, 1998; *Ohtani et al.*, 1998, 1999, and references therein]. On the basis of this idea we have investigated the temporal and spatial evolution of the near-Earth magnetotail in order to study the substorm onset triggering with emphasis on the cause-and-effect rela-

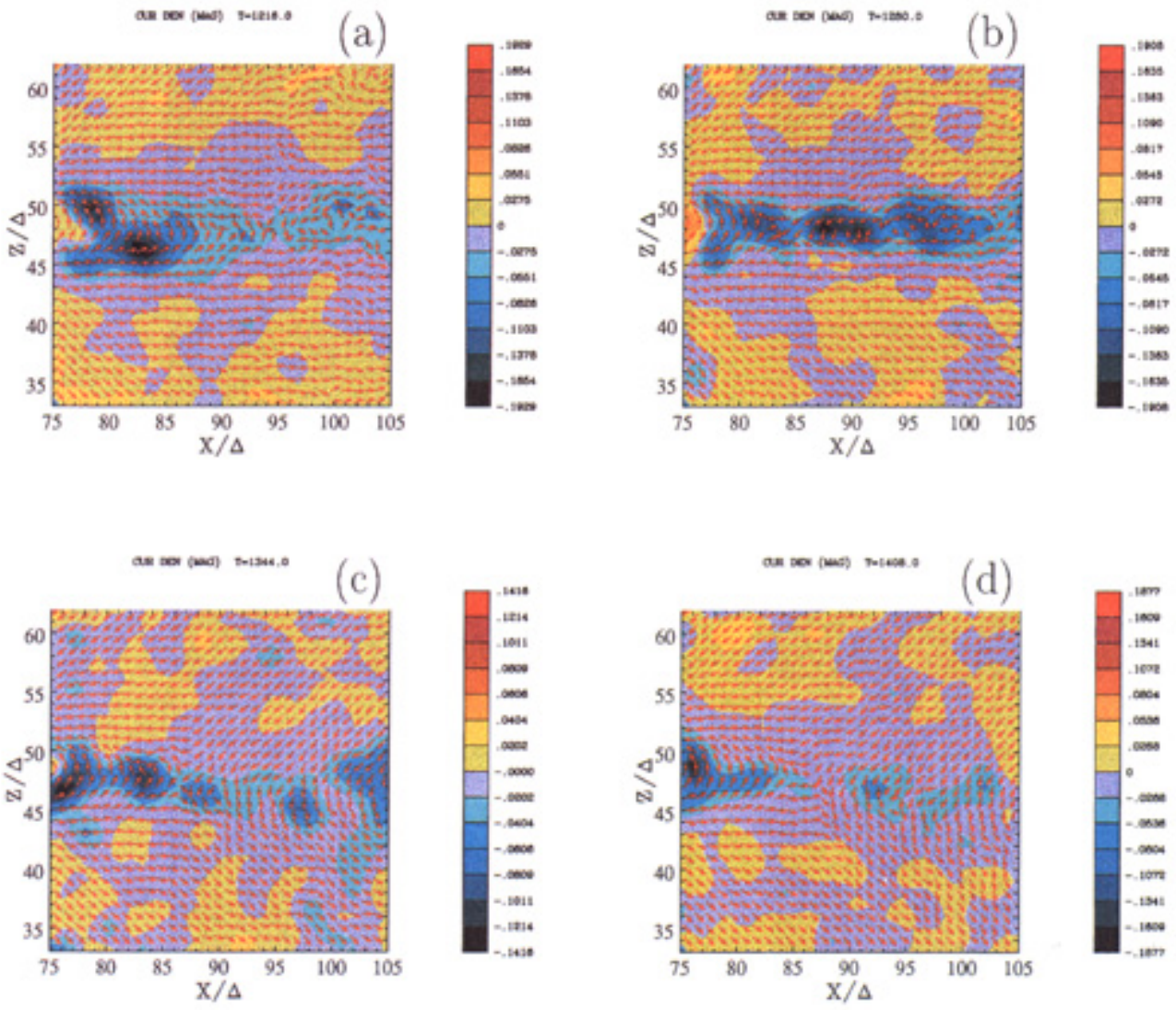

Plate 1. Current density J_y in the noon-midnight meridian cross section at time step (a) 1216, (b) 1280, (c) 1344, and (d) 1408. The arrows show the magnetic field.

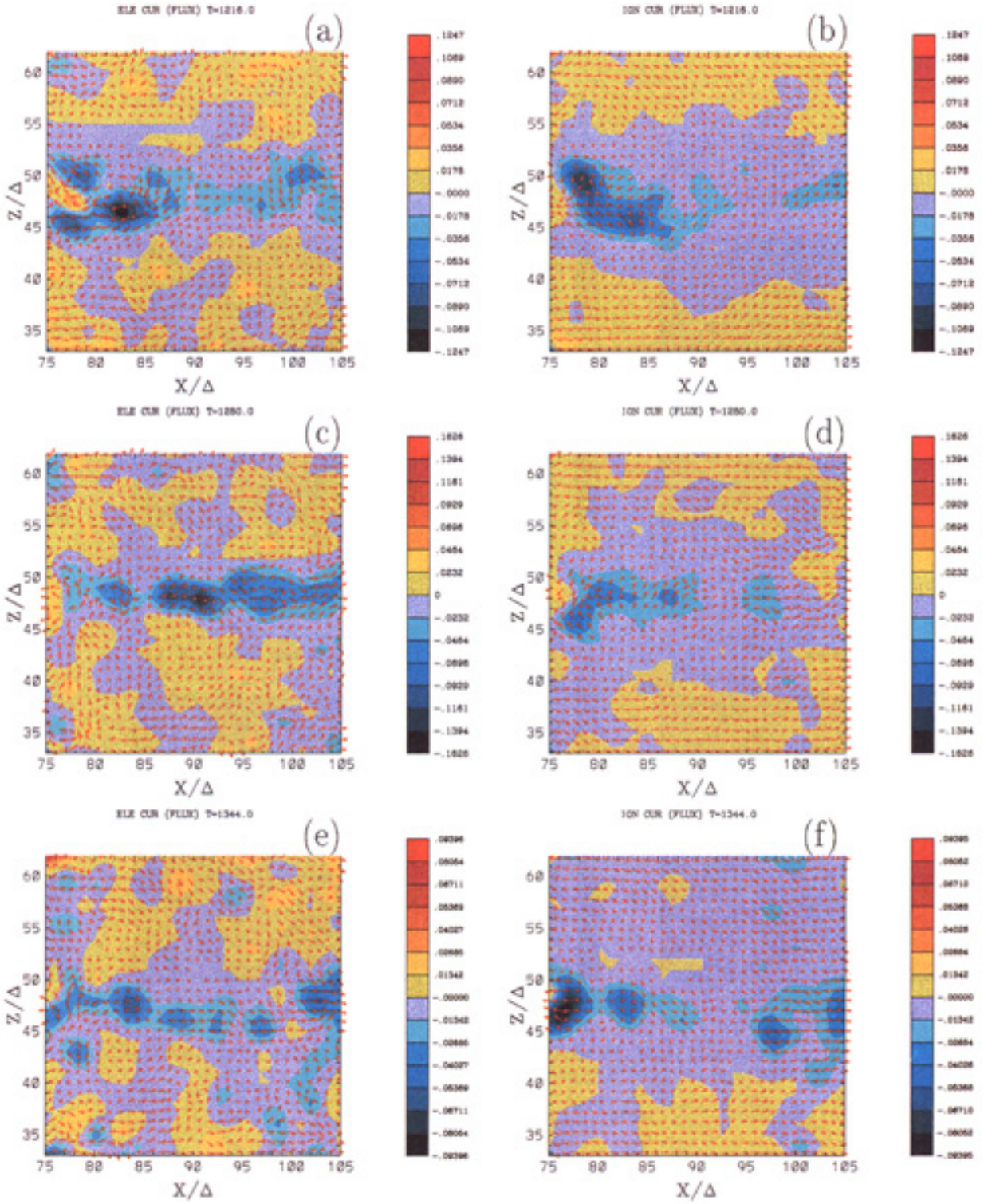

Plate 2. Comparison of (a), (c), and (e) electron and (b), (d), and (f) ion current in the noon-midnight meridian cross section at time steps 1216 (Plate 2a and 2b), 1280 (Plate 2c and 2d), and 1344 (Plate 2e and 2f). The arrows show its flux. For each time step the same scale is used.

tionship among the formation of a near-Earth neutral line (NENL), earthward plasma flows, and the trigger of tail current disruption. New studies show that the peak of current density moves toward the Earth. Before its peak becomes maximum the reconnection takes place. The earthward flows are generated by the reconnection, which leads to the earthward expansion of the intensified sheet current. The pileup of the earthward plasma flows generates the dawnward current near the Earth. This dawnward current coalesces with the sheet current because of the opposite current direction in the near-Earth tail, which coincides with the dipolarization. This simulation study shows the sequence of the substorm dynamics in the near-Earth tail. The identification of the timing and mechanism of triggering substorm onset will be done in a subsequent study. In section 2 we summarize the previous studies and describe new findings. The concluding remarks and future studies are discussed in section 3.

2. Simulation Models and Results

The increase of available core memory and speed on supercomputers such as the CRAY C90 and T90 now enables us to perform 3-D particle simulations with reasonably realistic parameters. We use a 3-D electromagnetic particle code [*Buneman*, 1993]. This code utilizes charge-conserving formulas [*Villasenor and Buneman*, 1992] and radiating boundary conditions [*Lindman*, 1975].

For the simulation of solar wind-magnetosphere interactions the following boundary conditions were used for the particles [*Buneman et al.*, 1992, 1995: *Nishikawa et al.*, 1995; *Nishikawa*, 1997, 1998a, b]: (1) Fresh particles representing the incoming solar wind (unmagnetized in our test run) are continuously injected across the $y-z$ plane at $x = x_{\min}$, and a thermal particle flux is also injected across the sides of our rectangular computation domain; (2) escaping particles are arrested in a buffer zone, redistributed there more uniformly by making the zone conducting in order to simulate their escape to infinity, and finally written off. We use a simple model for the ionosphere where both electrons and ions are reflected by the Earth's dipole magnetic field. Effects of a conducting ionospheric boundary will be developed in future simulations. The effects of the Earth's rotation are not included.

For the fields, boundary conditions were imposed just outside these zones [*Buneman et al.*, 1992, 1995: *Nishikawa et al.*, 1995, *Nishikawa*, 1997, 1998a, b]: radiation is prevented from being reflected back inward, following Lindman's [1975] ideas. The lowest-order Lindman approximation was found to be adequate: radiation at glancing angles was no problem. However, special attention was given to conditions on the edges of the computational box.

In order to bring naturally disparate timescales and space scales closer together in this simulation of phenomena dominated by ion inertia and magnetic field interaction the natural electron mass was raised to one sixteenth of the ion mass, and the velocity of light was lowered to twice the incoming solar wind velocity. This means that charge separation and anomalous resistivity phenomena are accounted for qualitatively but perhaps not with quantitative certainty. Likewise, radiation-related phenomena (e.g., whistler modes) are covered qualitatively only.

Initially, ~ 2 million electron-ion pairs fill the entire box (215 by 95 by 95; the effective number of cells, 1.7 million) uniformly and drift with a velocity $v_{\rm sol} = 0.5c$ in the $+x$ direction, representing the solar wind without an IMF. The electron and ion thermal velocities are $v_{et} = (T_e/m_e)^{1/2} = 0.2c$ and $v_{it} = (T_i/m_i)^{1/2} = 0.05c\,(= v_s = (T_e/m_i)^{1/2})$, respectively, while the magnetic field is initially zero. A circular current generating the dipole magnetic field is increased smoothly from 0 to a maximum value reached at time step 65 and kept constant at that value for the rest of the simulation, which maintains the steady dipole magnetic field. The center of the current loop (the Earth) is located at $(70.5\Delta, 47.5\Delta, 48\Delta)$ with the current in the $x-y$ plane and the axis in the z direction. The initial expansion of the magnetic field cavity is found to expel a large fraction of the initial plasma. The injected solar wind density is ~ 0.8 electron-ion pairs per cell, the mass ratio is $m_i/m_e = 16$ and $\omega_{pe}\Delta t = 0.84$.

The results of an unmagnetized solar wind plasma streaming past a dipole magnetic field show the formation of a magnetopause and a magnetotail, the penetration of energetic particles into cusps, and radiation belt and dawn-dusk asymmetries [*Buneman et al.*, 1992, 1995; *Nishikawa et al.*, 1995]. After a quasi-steady state is established with an unmagnetized solar wind, at time step 768 [*Buneman et al.*, 1995; *Nishikawa et al.*, 1995] a southward IMF ($B_z^{\rm IMF} = -0.4$) is switched on gradually (for comparison, the average B_z at the dayside magnetopause ($\approx 10R_{\rm E}$) is nearly 2.8), and the southward IMF front reaches about $x = 120\Delta\,(\approx -50R_{\rm E})$ at time step 1280. The Alfvén velocity with this IMF is $v_A/c = 0.1(\bar{n}_i)^{-1/2} = 0.1$ for the average ion density $\bar{n}_i = 1$ [*Nishikawa*, 1997, 1998a].

Plate 1 shows the evolution of the thinned current sheet with a southward IMF [*Nishikawa*, 1997, 1998a]. At time step 1216 (the front of the solar wind with the southward IMF reaches at $x = 104\Delta\,(\approx -34R_{\rm E})$) the magnetic field is thinned and the current density is intensified near the Earth ($x < 87\Delta$) as is shown in Plate 1a (see also Plate 4b) because of the duskward electric field ($E_y \approx -v_{\rm sol} \times B_{\rm IMF}$). The intensified current density extends deeper in the tail as the southward IMF moves toward the distant tail. At time step 1280 the reconnection takes place at $x = 85\Delta(\approx -15R_{\rm E}$ (see also Plate 4c). Because of the reconnection and the plasmoid (see Plate 4d) the high current density shifts toward the Earth and the distant tail (Plate 1c). Then, the current sheet is localized near the Earth as shown in Plate 1d.

The comparison of electron and ion currents is shown in Plate 2. The electron current (Plate 2a, 2c, and 2e) and ion current (Plate 2b, 2d, and 2f) are plotted with the normalized maximum and minimum current density for each time step (Plate 2a and 2b: 1216; Plate 2c and 2d: 1280; and Plate 2e and 2f: 1344) at $y = 0.0R_E$. It should be noted that since the current density is averaged over the current sheet in Figure 1, both values in Plate 2 and Figure 1 are not necessarily matched. It is clear that near the Earth the dominant current carriers are ions. However, electron currents play a role near the reconnection region (around $(x, z) = (86\Delta, 48\Delta) \approx (-16R_E, 0R_E)$). Since the gyroradius of electrons is smaller than that of ions, electrons are magnetized in the reconnection regions [*Hesse et al.*, 1996]. On the other hand, ions are not magnetized in the reconnection region. The arrows show its flux Σv_j. Particles are ejected toward the Earth from the reconnection region [e.g., *Lopez et al.*, 1994; *Sergeev et al.*, 1995; *Angelopoulos et al.*, 1996; *Shiokawa et al.*, 1997].

In order to visualize the evolution of the current sheet the averaged current density with the separated electron (uneven dashed curves) and ion (dashed curves) currents is plotted along the x direction at time step 1088, 1152, 1216, 1280, and 1344 as shown in Figure 1. The current is averaged over $2R_E \geq z \geq -2R_E$ and $3.5R_E \geq y \geq -3.5R_E$. The average current density (duskward: plus) is multiplied by 100, and 15 is added at each time step (for example, 30 is 0.0 for time step 1216). The current profile at 1088 shows the current sheet without the southward IMF (with the unmagnetized solar wind, the solar wind with the southward IMF has not arrived yet at the tail). At time step 1152 the southward IMF begins to enhance the current density [*Kaufmann*, 1987; *Pulkkinen et al.*, 1991]. The current sheet is thinned as shown in Plate 1a at time step 1216. The peaks are located at $x = 79\Delta(\approx -9R_E)$ at both time steps. The dawnward current is generated at time step 1216, and it increases at time step 1280. It disappears at 1344 with the dipolarization. Among these time steps the maximum current density is found at 1216, which is ~ 3 times larger than that without the southward IMF at time step 1088 (unmagnetized solar wind). Before time step 1280 the reconnection occurs at $x = 85\Delta(\approx -15R_E)$. The local minimum in the current density (at $x = -15R_E$) is created by the ejection of particles from the reconnection region. Because of the ejection by the reconnection, particles are injected into the magnetosphere, and the peaks of the current density also move toward the Earth as seen at time steps 1216, 1280, and 1344. Because of this earthward movement of the peak current density, the local current density decreases (at $x = 80\Delta(\approx -10R_E)$), which is related to the local current disruption [*Ohtani et al.*, 1999]. The earthward movement of the peak value in the current density is consistent with the observations of the earthward expansion of the current disruptions [*Ohtani*, 1998; *Ohtani et al.*, 1999].

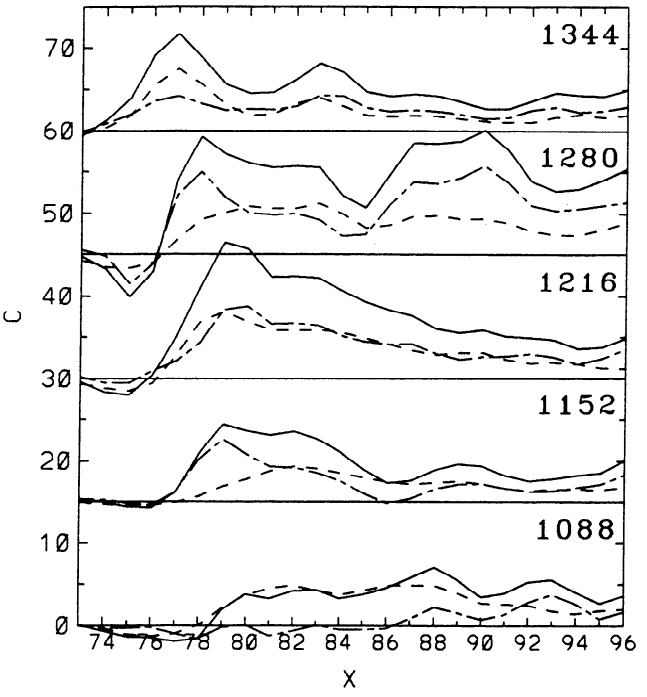

Figure 1. Evolution of the averaged current sheet ($2R_E \geq z \geq -2R_E$, $3.5R_E \geq y \geq -3.5R_E$) is plotted along the x direction with the electron (the uneven dashed curve) and ion (dashed curve) currents at time steps 1088, 1152, 1216, 1280, and 1344. Before the reconnection the current becomes maximum with thinning at $x = 79\Delta(\approx -9R_E)$. At 1216 the electron and ion currents are very similar. The electron current becomes larger than the ion one at $x = 78\Delta(\approx -8R_E)$. However, at 1344 the ion current is twice as large as than the electron one at $x = 77\Delta(\approx -7R_E)$.

The gradient of current sheet becomes very steep at time step 1280. It is proposed that the wedge current is generated by the dawnward inertia current [e.g., *Haerendel*, 1992; *Shiokawa et al.*, 1997, 1998a]. (Since a simple ionospheric model is used in our present model (particles are reflected by the mirror force), the investigation of the wedge current is out of the scope of our simulation study.) However, the inertia current is not the driving force of the full substorm current circuit during the expansion and recovery phases [*Shiokawa et al.*, 1998b] since the high-speed flows last only for several minutes [*Baumjohann et al.*, 1990; *Angelopoulos et al.*, 1992, 1994]. On the basis of Figure 1, since the current density takes the maximum value before the reconnection, the kinetic instability (cross-field current instability) takes place prior to the reconnection. *Daughton* [1998, 1999] has investigated the stability of the drift kinetic instability with a Harris-type equilibrium using a kinetic description for both ions and electrons. It is difficult to identify the instability that is responsible for exciting reconnection [*Lapenta and Brackbill*, 1997; *Daughton*, 1998, 1999; *Nishikawa*, 1997, 1998a]. It requires further investigation with better resolutions and

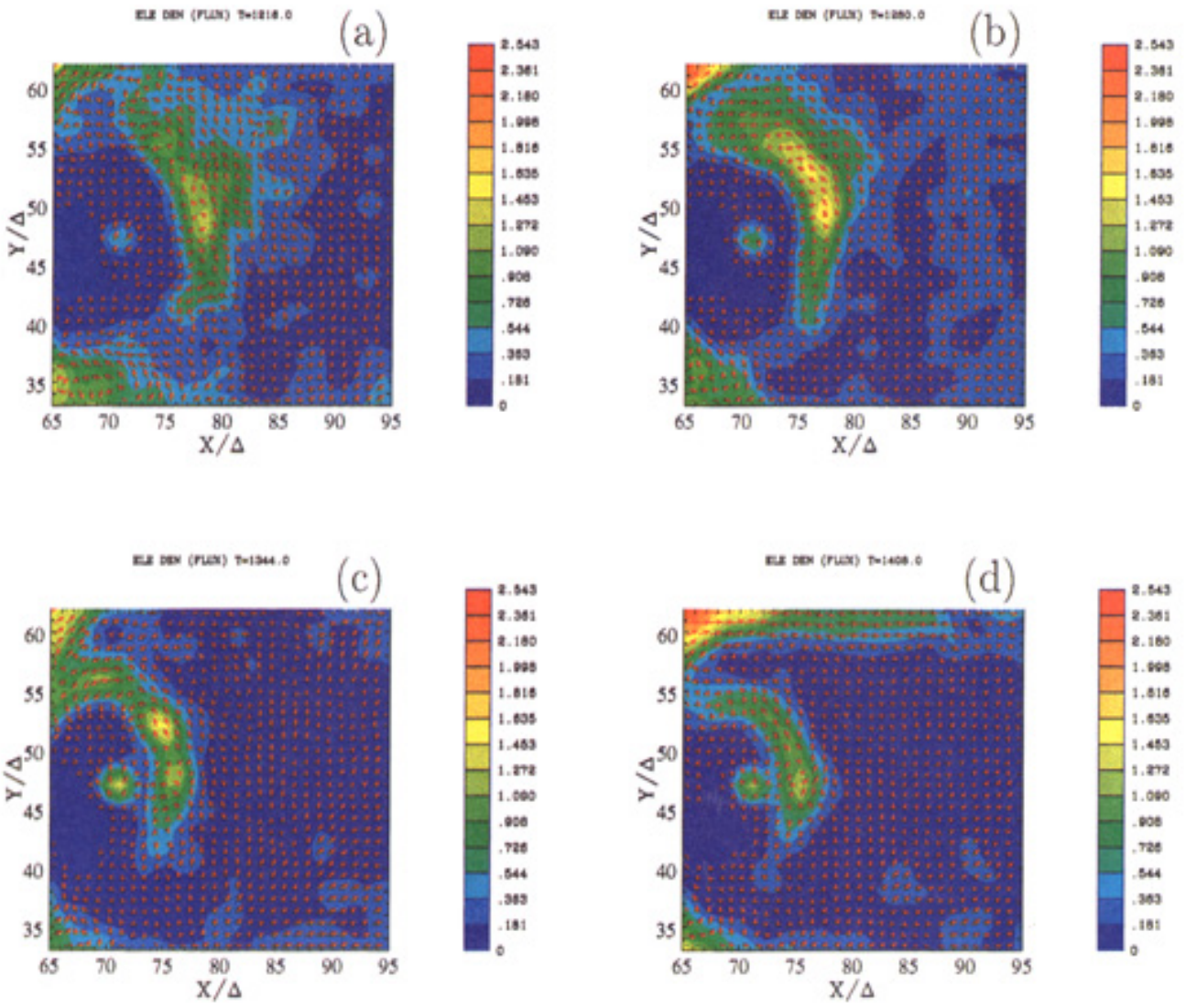

Plate 3. Injection of electrons (ions) into the near Earth caused by the reconnection as shown in the equatorial plane at time (a) 1216, (b) 1280, (c) 1344, and (d) 1408. The arrows show electron flux.

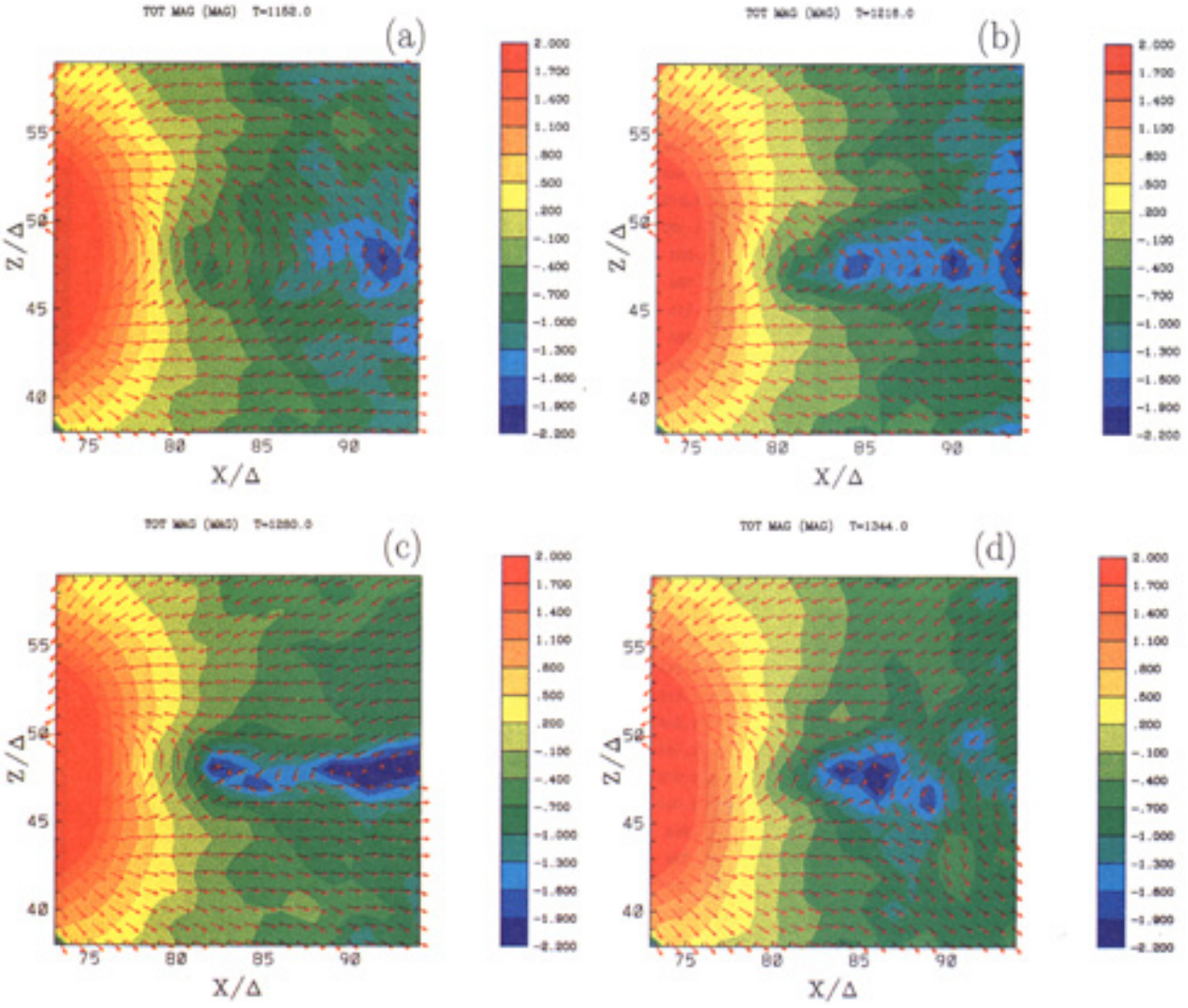

Plate 4. Magnetic field strength in the $x - z$ plane in the near-Earth magnetotail at time steps (a) 1152, (b) 1216, (c) 1280, and (d) 1344. The arrows show the magnetic field.

larger mass ratios to identify the instability with the thinned current sheet.

In order to examine the dawnward current the evolution of electron density in the equatorial plane is plotted at time steps (a) 1216, (b) 1280, (c) 1344, and (d) 1408 near the Earth in Plate 3 (the maximum density is normalized for Plate 3a - 3d). The ion density is very similar to the electron density. As shown in Figure 1 at time step 1280, the dawnward current becomes maximum around $x = 75\Delta(\approx -5R_{\rm E})$, which is consistent with the maximum density gradient around $x = 75\Delta$ (near the subsolar line ($y = 47\Delta$)) in Plate 3b. Therefore the dawnward current is generated by the pressure (density) gradient [e.g., *Park*, 1991; *Birn et al.*, 1999]. At a later time (Plate 3c) the density gradient becomes smaller, which is consistent with the banished dawnward current (at time 1344) in Figure 1.

The dipolarization is one of the processes that is closely related to the wedge current [e.g., *Kan*, 1998; *Ohtani et al.*, 1999]. Total magnetic field strength ($\log(|\mathbf{B}(x,y,z)|)$ at $y = 47\Delta$) in the noon-midnight cross-section ($x - z$) plane in the near-Earth magnetotail is plotted at time steps (a) 1152, (b) 1216, (c) 1280, and (d) 1344 in Plate 4. In Plate 4a - 4d the maximum and minimum values are set in order to highlight the changes due to reconnection and the dipolarization of the magnetotail. The arrows show the magnetic field (renormalized to show the weaker magnetic field). At time step 1152 (Plate 4a) the arrows show an ordinary stretched dipole magnetic field. The further stretching of the magnetic field is found in the weakening normal component (B_z) (still positive) in the central sheet (Plate 4b). At time step 1280 the x point is created, which shows the occurrence of reconnection around $x = 85\Delta(\approx -15R_E)$ as shown in Plate 4c. Because of the reconnection, the normal z components become negative ($83\Delta < x < 90\Delta$) in the central sheet. At the same time the local dipolarization is found around $x = 80\Delta$ (it is more easily recognized with a vertical line at $x = 80\Delta$). The boundary line at value -0.4 moves toward the tail at time step 1280. This comes from the magnetic transfer by the reconnection. Further dipolarization takes place in the near-Earth magnetotail as shown in Plate 4d. The evidence of dipolarization is subtle, therefore careful attention needs to be paid to recognize it. The dipolarization is recognized in two ways. First, the weak magnetic field region with dark blue created by the reconnection around $x = 82\Delta, z = 48\Delta$ in Plate 4c moves tailward in Plate 4d ($x = 84\Delta, z = 48\Delta$). Second, the negative B_z components on the subsolar line ($z = 48\Delta$) ($83\Delta \geq x \geq 85\Delta$) (Plate 4c) become positive in Plate 4d (this is viewed easily using magnification by ghostview). Furthermore, the detailed analysis shows that the boundary at the value of 0.200 (yellow-yellowish green), which is bowed toward the Earth at the subsolar line (Plate 4c) becomes more straight (less bowed) because of the dipolarization in Plate 4d (it is more easily recognized with a vertical line at $x = 79\Delta$). As shown in Figure 1, the dipolarization coincides with the current decrease at time step 1344.

3. Discussion

The evolution of thinned cross-field current with a southward IMF is studied in order to address the cause-and-effect relationship between the reconnection and the current disruption. The southward IMF drives the complicated processes in the near-Earth magnetotail as shown in the previous section. Our 3-D global EM particle simulation results show that the cross-field current is enhanced at the substorm growth phase with a southward IMF. It is important to determine the current carrier in the thinned current sheet including effects from the magnetopause and (lower-latitude) boundary layers using a global system (not local simulations). The evolution of the averaged current density is studied as a function of x. The current profile at 1088 shows the current sheet without the effects of southward IMF (with the unmagnetized solar wind). At 1152 the duskward electric field accompanied by the southward IMF begins to enhance the current sheet in the near-Earth magnetotail ($78\Delta < x < 84\Delta$) ($-8R_{\rm E} > x > -14R_{\rm E}$). The current sheet is thinned at time step 1216. The peaks of the current density are located at $x = 79\Delta(\approx -9R_{\rm E})$ at both time steps. The intensified current density excites a kinetic instability that is not yet fully understood [*Daughton*, 1998, 1999; *Nishikawa*, 1997, 1998a, references therein]. Because of the instability excited by the thinned current sheet, the stabilization effects of normal component B_z [e.g., *Pellat et al.*, 1991] are eliminated, and the reconnection takes place [e.g., *Nishikawa*, 1997, 1998a]. The dawnward current is generated by the pressure gradient drift at 1216, and it increases at time step 1280. It disappears at time step 1344 with the dipolarization. Among these time steps the maximum current density at $x = 79\Delta(\approx -9R_{\rm E})$ is found at 1216, which is ~ 3 times larger than that without the southward IMF before the reconnection takes place. Around time step 1280 the reconnection occurs, which is identified in the gap of current density at $x = 85\Delta(\approx -15R_{\rm E})$. This local minimum of the current density is created by the ejection of particles from the reconnection region ($x = 85\Delta$). Because of the ejection of particles by the reconnection, particles are injected into the inner magnetosphere and the peaks of current density also move toward the Earth as seen at time steps 1216, 1280, and 1344. This may be related to the observations of the earthward expansion of the current disruptions [*Ohtani*, 1998; *Ohtani et al.*, 1999]. The gradient of current density near the Earth ($-5R_{\rm E} > x > -8R_{\rm E}$) becomes very steep at time step 1280. Because of the opposite current direction between the dawnward current and the cross-field current they decrease rapidly with the dipolarization.

Because of the reconnection, the particles are ejected

from the reconnection region, and the structure of the current sheet is changed. The current carriers are checked, and ions become dominant near the Earth. At the time when reconnection occurs, electrons become major carriers near the reconnection region. After the reconnection, ions become the dominant carrier. The dawnward current is observed, which may be responsive to the wedge current. In the near-Earth plasma sheet, (high-speed) ion flow is observed, which is generated by the reconnection. At the same time the dipolarization is observed as shown in Plate 4. On the basis of these simulation results we believe that the current disruption is at least one of the triggering mechanisms of substorms. However, as shown in this paper, the processes are so complicated and so many phenomena are involved that we need further investigation in order to understand the evolution of thinned cross-field current before the onset of substorms. In order to investigate wedge current we need to implement better ionosphere than the present simple cusp ionosphere (particles are reflected by the mirror force with some drifts due to an induced electric field). Inclusion of injected ionosphere particles will also be necessary to account for the ionosphere. We will report it in the future.

In order to examine the current system in the center of the near-Earth and midtail the current stream lines are traced from the subsolar line ($y = z = 0.0R_E$) toward the dawn (positive) and dusk (negative) at time step 1280. The stream lines start from at $x = -4.0, -4.5,$ - - -, -19.0, and $19.5R_E$ (30 points). The current stream lines are traced in the 3-D current vectors. Figure 2 shows current stream lines in the three different projections (a) $x - z$ (noon-midnight), (b) $y - z$ (dusk-dawn), and (c) $x-y$ (equatorial) planes. (The iterations are stopped after 500 steps and/or the vales of current density are too small to be traced.) Figure 2c shows that in general, the current flows from the dawnside ($y \approx -13R_E$) to the duskside ($y \approx 15R_E$) in the equatorial plane ($x < -9R_E$). It should be noted that the sheet current is curved toward the Earth in the postmidnight sector ($0 > y > -12R_E$, $0 > x > -12R_E$). In the premidnight sector ($x < -8R_E$) the sheet currents (duskward) are connected to the dawnward current. This shows that the current system near the Earth is altered from the simple tail current because of the generation of the dawnward current and probably field-aligned (wedge) currents [*Birn et al.*, 1999]. Figure 2b shows that at both the dawnside ($y \approx -13R_E$) and duskside ($y \approx 15R_E$) most of the sheet currents are connected to the magnetopause currents (few current stream lines are lost in the magnetosheath).

Recently, *Ohtani et al.* [1999] have examined the timing of various onset-associated signatures and the cause-and-effect relationship between the formation of a NENL and the trigger of tail current disruption with multisatellite observations. In the December 31, 1995, event (the IMF B_z was ~ -5 nT for the most of the interval except for a few short periods) a NENL was formed after the initial tail current intensification [see *Ohtani et al.*, 1999, Figure 15]. Further, tail current intensification takes place after the reconnection. At the near-Earth tail the tail current disrupts (in our simulation the current decreases (at time step 1344)). This fundamental sequence is similar to our simulation results described in section 2.

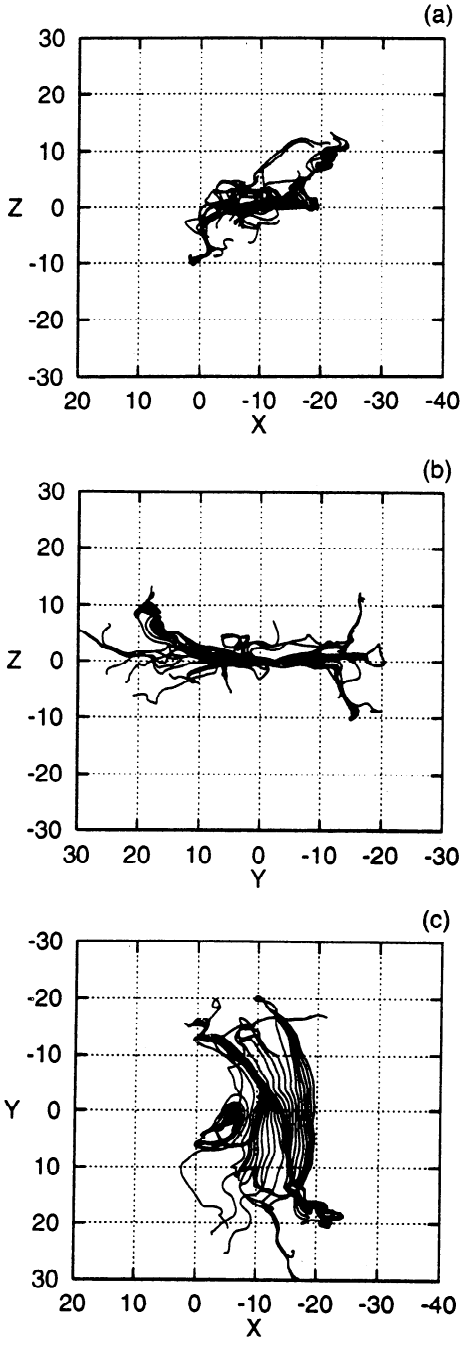

Figure 2. Current lines through the subsolar line are plotted in (a) the $x - z$ plane, (b) $y - z$ plane, and (c) $x - y$ plane at time step 1280. The current flows from the dawnside to the duskside.

The results reported here suggest that full 3-D electromagnetic particle simulations will become an important tool for the theoretical understanding of Earth's

magnetosphere in the not-so-distant future. It is clearly necessary to use more realistic values of m_i/m_e with a larger system and more particles in a cell, which relies on the development of future more powerful and faster supercomputers. This would help to establish more precisely the nature of the magnetic reconnection and associated phenomena and to clarify their relation to the observations. For the present, however, scaling and grid size remain substantial problems. For example, in our simulation the Debye length and the thickness of the bow shock are both of the order of an Earth radius, which is of the order of a grid spacing. However, some form of scaling is usually needed in particle simulations, even in one and two dimensions, and still, such simulations are able to reveal much of the physics behind natural phenomena. Further, simulations including time-dependent IMFs (including B_x and B_y) and transient shocks are in progress and will be reported elsewhere.

Although our simulation studies have shown the sequence of the tail dynamics, which is similar to the observations [*Ohtani et al.*, 1999], further investigations need to be studied in order to understand better the triggering mechanism of substorms. We will report further progress in a separate paper.

Acknowledgments. Support for this work was provided by NSF grants ATM-9730230 and ATM-9996266. The development of the simulation code was performed at the National Center for Supercomputing Applications, University of Illinois at Urbana-Champaign, and the production runs were performed at Pittsburgh Supercomputing Center. The postanalysis of simulations has been made at San Diego Supercomputing Center. All centers are supported by the National Science Foundation.

Janet G. Luhmann thanks the referees for their assistance in evaluating this paper.

References

Angelopoulos, V., The role of impulsive particle acceleration in magnetotail circulation, in *Proceedings of the Third International Conference on Substorms (ICS-3), Eur. Space Agency Spec. Publ., ESA SP-389*, p. 17, 1996.

Angelopoulos, V., W. Baumjohann, C. F. Kennel, F. V. Coroniti, M. G. Kivelson, R. Pellat, R. J. Walker, H. Lühr, and G. Paschmann, Bursty bulk flows in the inner central plasma sheet, *J. Geophys. Res., 97*, 4027, 1992.

Angelopoulos, V., C. F. Kennel, F. V. Coroniti, R. Pellat, M. G. Kivelson, R. J. Walker, C. T. Russell, W. Baumjohann, W. C. Feldman, and J. T. Gosling, Statistical characteristics of bursty bulky flow events, *J. Geophys. Res., 99*, 21,257, 1994.

Baker, D. N., T. I. Pulkkinen, V. Angelopoulos, W. Baumjohann, and R. L. McPherron, Neutral line model of substorms: Past results and present views, *J. Geophys. Res., 101*, 12,975, 1996.

Baumjohann, W., G. Paschmann, and H. Lühr, Characteristics of high-speed ion flows in the plasma sheet, *J. Geophys. Res., 95*, 3801, 1990.

Birn, J., and M. Hesse, Details of current disruption and diversion in simulations of magnetotail dynamics, *J. Geophys. Res., 101*, 15,345, 1996.

Birn, J., M. Hesse, G. Haerendel, W. Baumjohann, and K. Shiokawa, Flow braking and the substorm current wedge, *J. Geophys. Res., 104*, 19,905, 1999.

Buneman, O., TRISTAN: The 3-D E-M Particle Code, in *Computer Space Plasma Physics: Simulation Techniques and Software*, edited by H. Matsumoto and Y. Omura, p. 67, Terra Sci., Tokyo, 1993.

Buneman, O, T. Neubert, and K.-I. Nishikawa, Solar wind-magnetosphere interaction as simulated by a 3-D E-M particle code, *IEEE Trans. Plasma Sci., 20*, 810, 1992.

Buneman, O, K.-I. Nishikawa, and T. Neubert, Solar wind-magnetosphere interaction as simulated by a 3-D E-M particle code, in *Space Plasmas: Coupling Between Samall and Medium Scale Processes, Geophys. Monogr. Ser.*, vol. 86, edited by M. Ashour-Abdalla, T. Chang, and P. Dusenbery, p. 347, AGU, Washington, D. C., 1995.

Daughton, W., Kinetic theory of the drift kink instability in a current sheet, *J. Geophys. Res., 103*, 29,429, 1998.

Daughton, W., The unstable eighenmodes of a neutral sheet, *Phys. Plasmas, 6*, 1329, 1999.

Fairfield, D. H., Advances in magnetospheric storm and substorm research: 1989-1991, *J. Geophys. Res., 97*, 10,865, 1992.

Galeev, V. K., and L. M. Zelenyi, Tearing instability in plasma configuration, *Sov. Phys. JETP*, Engl. Transl., *43*, 1113, 1976.

Haerendel, G., Disruption, ballooning, or auroral avalanche: On the cause of substorms. in *Proceedings of the 1st International Conference on Substorms (ICS-1)*, p. 417, Eur. Space Agency, Kiruna, Sweden, 1992.

Hesse, M., and J. Birn, On dipolarization and its relation to the substorm current wedge, *J. Geophys. Res., 96*, 19,417, 1991.

Hesse, M., D. Winske, M. Kuznetsova, J. Birn, and K. Schindler, Hybrid modeling of the formation of thin current sheet in magnetotail configurations, *J. Geomagn. Geoelectro., 48*, 749, 1996.

Kan, J. R., A globally integrated substorm model: Tail reconnection and magnetosphere-ionosphere coupling, *J. Geophys. Res., 103*, 11,787, 1998.

Kaufmann, R. L., Substorm currents: Growth phase and onset, *J. Geophys. Res., 92*, 7471, 1987.

Lapenta, G., and J. U. Brackbill, A kinetic theory for the drift-kinetic instability, *J. Geophys. Res., 102*, 27,099, 1997.

Lembège, B., and R. Pellat, Stability of a thick two-dimensional quasineutral sheet, *Phys. Fluids, 25*, 1995, 1982.

Lindman, E. L., "Free-space" boundary conditions for the time dependent wave equation, *J. Comput. Phys., 18*, 66, 1975.

Lopez, R. E., C. C. Goodrich, G. D. Reefves, R. D. Belian, and A. Taktakishvili, Midtail plasma flows and the relationship to near-Earth substorm activity, *J. Geophys. Res., 99*, 23,561, 1994.

Lui, A. T. Y., A synthesis of magnetospheric substorm models, *J. Geophys. Res., 96*, 1849, 1991.

Lui, A. T. Y., R. E. Lopez, B. J. Anderson, K. Takahashi, L. J. Zanetti, R. W. McEntire, T. A. Potemra, D. M. Klumpar, E. M. Greene, and R. Strangeway, current disruptions in the near-Earth neutral sheet region, *J. Geophys. Res., 97*, 1461, 1992.

Ma, Z. W., X. Wang, and A. Bhattacharjee, Growth, sudden enhancement, and relaxation of current sheets in the magnetotail: Two-dimensional substorm dynamics, *Geophys. Res. Lett., 22*, 2985, 1995.

Mitchell, D. G., D. J. Williams, C. Y. Huang, L. A. Frank, and C. T. Russell, Current carriers in the near-Earth cross-tail current sheet during substorm growth phase, *Geophys. Res. Lett., 17*, 583, 1990.

Mukai, T., M. Hoshino, Y. Saito, I. Shinohara, and T. Yamamoto, Pre-onset and Onset signatures for substorms in the near-tail plasma sheet: Geotail observations, *Proceedings of the Fourth International Conference on Substorms (ICS-4)*, p. 131, Terra Scientific, Tokyo, 1998.

Nishikawa, K.-I., Particle entry into the magnetosphere with a southward IMF as simulated by a 3-D EM particle code, *J. Geophys. Res., 102*, 17,631, 1997.

Nishikawa, K.-I., Reconnections at near-Earth magnetotail and substorms studied by a 3-D EM particle code, in *Geospace Mass and Energy Flow: Results From the International Solar-Terrestrial Physics Program, Geophys. Monogr. Ser.*, vol. 104, edited by J. L. Horwitz, W. K. Peterson, and D. L. Gallagher, p. 175, AGU, Washington D. C., 1998a.

Nishikawa, K.-I., Particle entry through reconnection grooves in the magnetopause with a dawnward IMF as simulated by a 3-D EM particle code, *Geophys. Res. Lett., 25*, 1609, 1998b.

Nishikawa, K.-I., O. Buneman, and T. Neubert, Solar Wind-Magnetosphere Interaction as Simulated by a 3-D EM Particle Code, in *Plasma Astrophysics and Cosmology*, edited by A. T. Peratt, p. 265, Kluwer Acad. Norwell, Mass., 1995.

Ohtani, S., Earthward expansion of tail current disruption: Duel-satellite study, *J. Geophys. Res., 103*, 6815, 1998.

Ohtani, S., and T. Tamao, Does the ballooning instability trigger substorms in the magnetotail? *J. Geophys. Res., 98*, 19,369, 1993.

Ohtani, S., K. Takahashi, T, Higuchi, A. T. Y. Lui, H. E. Spence, and J. F. Fennell, AMPTE/ CCE-SCATHA simultaneous observations of substorm-associated magnetic fluctuations, *J. Geophys. Res., 103*, 4671, 1998.

Ohtani, S., F. Creutzberg, T. Mukai, H. Singer, A. T. Y. Lui, M. Nakamura, P. Prikyl, K. Yumoto, and G. Rostoker, Substorm oneset timing: The December 31, 1995, event, *J. Geophys. Res., 104*, 22,713, 1999.

Park, G. K., *Physics of Space Plasmas: An Introduction*, Addison-Wesley-Longman, Reading, Mass., 1991.

Pellat, R., F. V. Coroniti, and P. L. Pritchett, Does ion tearing exist?, *Geophys. Res. Lett., 18*, 143, 1991.

Pritchett, P. L., Effect of electron dynamics on collisionless reconnection in two-dimensional magnetotail equilibria, *J. Geophys. Res., 99*, 5935, 1994.

Pritchett, P. L., and J. Büchner, Collisionless reconnection with a minimum in the equatorial magnetic field and with magnetic shear, *J. Geophys. Res., 100*, 3601, 1995.

Pritchett, P. L., and F. V. Coroniti, Formation of thin current sheets during plasma sheet convection, *J. Geophys. Res., 100*, 23,551, 1995.

Pritchett, P. L., and F. V. Coroniti, The role of the drift kink modes in destabilizing thin current sheets, *J. Geomagn. Geoelectro., 48*, 833, 1996.

Pritchett, P. L. and F. V. Coroniti, Interchange and kink modes in the near-Earth plasma sheet and their associates plasma flows, *Geophys. Res. Lett., 22*, 2925, 1997.

Pritchett, P. L., F. V. Coroniti and V. K. Decyk, Three-dimensional stability of thin quasi-neutral current sheets, *J. Geophys. Res., 101*, 27,413, 1996.

Pritchett, P. L., F. V. Coroniti, and R. Pellat, Convection-driven reconnection and the stability of the near-Earth plasma sheet, *Geophys. Res. Lett., 24*, 873, 1997.

Pulkkinen, T. I., D. N. Baker, D. H. Fairfield, R. J. Pellinen, J. S. Murphree, R. D. Elphinstone, R. L. McPherron, J. F. Fennell, R. E. Lopez, and T. Nagai, Modeling the growth phase of a substorm using the Tyganenko model and multi-spacecraft observations: CDAW-9, *Geophys. Res. Lett., 18*, 1963, 1991.

Rostoker, G., Phenomenology and physics of magnetospheric substorms, *J. Geophys. Res., 101*, 12,955, 1996.

Roux, A., S. Perraut, P. Robert, A. Morane, A. Pederson, A. Korth, G. Kremser, B. Aparicio, D. Rodgers, and R. Pellinen, Plasma sheet instability to the westward traveling surge, *J. Geophys. Res., 96*, 17,687, 1991.

Samson, J. C., A. K. MacAulay, R. Rankin, P. Frycz, I. Voronkov, and L. L Cogger, Substorm intensifications and resistive shear flow-ballooning instabilities in the near-Earth magnetotail, *Proceedings of the Third International Conference on Substorms (ICS-3), Eur. Space Agency Spec. Publ., ESA SP-389*, p. 399, 1996.

Schindler, K., On the role of irregularities in plasma entry into the magnetosphere, *J. Geophys. Res., 84*, 7257, 1979.

Sergeev, V. A., P. Tanskanen, K. Mursula, A. Korth, and R. C. Elphic, Current sheet thickness in the near-Earth plasma sheet during substorm growth phase, *J. Geophys. Res., 95*, 3819, 1990.

Sergeev, V. A., V. Angelopoulos, D. G. Mitchell, and C. T. Russell, In situ observations of magnetotail reconnection prior to the onset of a small substorm, *J. Geophys. Res., 100*, 19,121, 1995.

Sergeev, V. A., T. I. Pulkkinen, and R. J. Pellinen, Coupled-mode scenario for the magnetospheric dynamics, *J. Geophys. Res., 101*, 13,047, 1996.

Shiokawa, K., W. Baumjohann, and G. Haerendel, Braking of high-speed flows in the near-earth magnetotail. *Geophys. Res. Lett. 24*, 1179, 1997.

Shiokawa, K., et al., High-speed ion flow, substorm current wedge, and multiple Pi2 pulsations. *J. Geophys. Res., 103*, 4491, 1998a.

Shiokawa, K., G. Haerendel, and W. Baumjohann, Azimuthal pressure gradient as driving force of substorm currents, *Geophys. Res. Lett. 25*, 959, 1998b.

Villasenor, J., and O. Buneman, Rigorous charge conservation for local electromagnetic field solvers, *Comput. Phys. Commun., 69*, 306, 1992.

K.-I. Nishikawa, Department of Physics and Astronomy, Rutgers, The State University of New Jersey, 136 Frelinghuysen Road, Piscataway, NJ 08854-8019 (e-mail: kenichi@physics.rutgers.edu)

S. Ohtani, Applied Physics Laboratory, The Johns Hopkins University, Johns Hopkins Road, Laurel, MD 20723-6099 (e-mail: ohtani@fluxgate.jhuapl.edu)

(Received June 18, 1999; revised September 23, 1999; accepted November 23, 1999.)